Influence on the martensitic transformation of the β phase decomposition process in a Cu–Al–Ni shape memory alloy

2005 J. Phys.: Condens. Matter 17 4223

(http://iopscience.iop.org/0953-8984/17/26/019)

INSTITUTE OF PHYSICS PUBLISHING JOURNAL OF PHYSICS: CONDENSED MATTER

J. Phys.: Condens. Matter **17** (2005) 4223–4236 doi:10.1088/0953-8984/17/26/019

Influence on the martensitic transformation of the β phase decomposition process in a Cu–Al–Ni shape memory alloy

J I Pérez-Landazábal[1], **V Recarte and V Sánchez-Alarcos**

Departamento de Física, Universidad Pública de Navarra, Campus de Arrosadía s/n, 31006 Pamplona, Spain

E-mail: ipzlanda@unavarra.es

Received 20 May 2005
Published 17 June 2005
Online at stacks.iop.org/JPhysCM/17/4223

Abstract

The decomposition of the metastable β_3 phase and its influence on the martensitic transformation (MT) has been analysed in a Cu–14.37Al–4.2Ni (wt%) shape memory alloy processed by powder metallurgy by differential scanning calorimetry, resonant ultrasound spectroscopy and *in situ* neutron powder diffraction. The pro-eutectoid γ_1 precipitation, the $L2_1$ to B2 disordering process and the eutectoid decomposition have been observed during heating, followed by its subsequent dissolution at higher temperatures. The γ_1 precipitation limits high-temperature applications. The evolution of the kind of induced martensite, hysteresis and transformation temperatures has been analysed during the precipitation of the γ_1 phase. The elastic stresses stored during quenching and the ordering degree play an important role in the MT evolution below 300 °C. At higher temperatures, the γ_1 precipitation process induces an increase of the MT transformation temperatures and hysteresis.

1. Introduction

The development of new materials is a key issue for the world's technological advance. Thus, from the viewpoint of materials science, there has been an increasing attention in the development and research of the so-called 'smart materials' [1]. This new kind of (composite) materials appeared as a result of the synthesis of structural and functional materials combined with the integration of a control mechanism. Some of the most interesting materials that can be used in smart materials are shape memory alloys (SMAs). Several SMA families can be found, such as Ni–Ti, Cu–Zn–Al, Cu–Al–Ni, Fe–Mn–Si, ... [2]. The properties of these alloys can be changed and controlled by the thermomechanical processing of the material,

[1] Author to whom any correspondence should be addressed.

so that they display the desired properties. The most relevant mechanical properties, such as shape memory, superelastic and pseudoelastic effects, are related to the first-order displacive and diffusionless martensitic transformation (MT) between the metastable high-temperature β phase and the low-temperature martensite phase [3].

In particular, Cu–Al–Ni SMAs are being developed as high-temperature smart materials due to their capacity to be used both as sensors and actuators at temperatures near 200 °C, this being an advantage over Cu–Zn–Al and Ti–Ni alloys whose maximum working temperatures is 100 °C [3]. The disordered β phase is stable at high temperature and it has a V-shaped phase field limited by the eutectoid temperature [4]. In order to retain the β phase in a metastable state at low temperature the alloy must be quenched from 900 °C to room temperature. During quenching the β phase undergoes two successively ordering processes, at the nearest neighbours and at the next-nearest neighbours, respectively [5]. The resulting β_3 phase has an $L2_1$ ordered cubic structure [6]. On further cooling, the β_3 phase undergoes a diffusionless MT. The concentration of the alloy plays a dominant role in the kind of martensitic phase and in the temperatures of the martensitic phase transformation. As a consequence of the displaciveness of the MT, the martensitic phase inherits the atomic order of the high-temperature phase. The characteristics of the MT (kind of martensite, transformation temperatures, hysteresis...) are very sensitive to the order degree of the β_3 phase and the precipitation processes due to the metastable character of this phase [7–10]. This aspect is of special interest in these alloys for high-temperature applications. Overheating or long enough low-temperature thermal treatments lead to the precipitation of the stable α and γ_1 phases that deteriorate the MT. To guarantee a good and reliable behaviour of devices based on these alloys, the evolution of the order at high temperature, the limit of stability of the β phases and its influence on the thermoelastic martensitic transformation must be studied. The deformation produced by the lattice shear is stored as elastic energy [11]. Thus, in the transformation region there is a local equilibrium between the difference in chemical Gibbs free energy (between β and martensite phases) and the stored elastic energy and energy dissipated by the frictional forces [12]. The balance between the different energy terms determines the characteristics of the MT: transformation temperatures and transformation interval, hysteresis, kind of induced martensite [13, 14]. The presence of precipitates of a stable phase in the matrix can modify this energy balance in different ways, by creating new martensite nucleation points, changing the matrix composition, impeding the movement of martensite–β_3 interface.

The stability limit of the β_3 phase in hypereutectoid compositions, high aluminium content, is determined by the γ_1 phase which appears during heating as a primary precipitation previous to the eutectoid reaction [15, 16]. This is a γ brass, i.e. an ordered complex body-centred cubic phase [17]. In the Cu–Al–Ni system the crystallographic structure ($P\bar{4}3m$ space group) of the cubic γ_1 phase ($a = 8.7039$ Å) is described as a binary Cu_9Al_4 in phase diagrams [4], although its ternary structure has been recently determined [18]. The effects of the precipitation of the γ_1 phase on the MT have been the subject of several studies on ternary Cu-based SMAs [19–22].

Cu–Al–Ni alloys are brittle due to their very high elastic anisotropy ($A \sim 13$) and large grain size [23], and in general show poor mechanical properties. The improvement of their mechanical properties is closely related to the production of alloys with fine grain size. Powder metallurgy has been shown to be a good alternative method to the addition of grain refiners in order to obtain fine grain size Cu–Al–Ni SMAs [24, 25]. In the present work, the decomposition of the metastable β_3 phase and its influence on the MT has been analysed in a Cu–14.37Al–4.2Ni (wt%) SMA processed by powder metallurgy by differential scanning calorimetry (DSC), resonant ultrasound spectroscopy (RUS) and *in situ* neutron powder diffraction.

2. Experimental procedure

A Cu–14.37Al–4.2Ni (wt%) shape memory alloy obtained by powder metallurgy and hot isostatic pressure (HIP) [24, 25] was employed in this work. This procedure avoids preferential grain orientation problems for the subsequent powder diffraction and RUS measurements. The samples were treated at 900 °C for 30 min in argon atmosphere and quenched into ice-temperature water to obtain the β phase. In order to characterize the evolution of the microstructure during heating and the characteristics of the martensitic transformations, neutron diffraction (ND), DSC and RUS have been used.

Powder ND studies were performed at the D20 and D1B installations at the Institute Laue-Langevin. The neutron wavelengths were $\lambda = 1.3$ and 2 Å respectively. To identify the precipitation process, samples were heated at 8 °C min^{-1} from room temperature up to 800 °C and every spectrum was measured over 1 min. Low-temperature measurements were made to determine the structure of the martensitic phase. The Rietveld method [26, 27] was used to identify and quantitatively determine the precipitated mass fraction of phases present. The FullProf 2000 program [28, 29] was employed to carry out the Rietveld refinement.

DSC measurements in a TA 2920 equipment were carried out between room temperature and 700 °C at 8 °C min^{-1} to analyse the different precipitation processes. In addition, to study the evolution of the MT, DSC cooling–heating cycles through the MT after heating up to different temperatures were performed in a TA Q100 DSC. These thermal treatments were performed in the DSC at the same heating rate up to the different temperatures. No time was spent at the maximum temperature and the subsequent free cooling was performed inside the calorimeter.

RUS can be used to quantify the elastic properties of a wide range of solid-state materials by measuring their resonance spectra [30, 31]. The elastic constants are determined after fitting the experimental resonance frequencies of the sample with theoretical resonances predicted from the shape, mass and preliminary elastic constants. A DRS Inc.^{TM} Modulus II system was used to analyse the resonant ultrasonic spectrum. A rectangular parallelepiped of $1.7998 \times 2.0427 \times 3.0402\,\text{mm}^3$ and mass $= 0.078\,77$ g was used for the RUS technique. To fit the experimental spectrum to the theoretical one, parallelism and perpendicularity between the faces of the parallelepiped require precision of 1 μm mm^{-1}. The lack of preferential grain orientation allows us to consider the material as isotropic, and consequently its elastic behaviour is defined by the elastic constants C_{11} and C_{44}. The measurements of elastic constants were performed at room temperature using a small sample holder provided by DRS. The frequencies of the lowest 30 resonances were measured with a typical rms difference between measured and computed frequencies of 0.2% or less. In order to compare with DSC and ND the sample was heated to different maximum temperatures with the same heating rate into the calorimeter and subsequently measured at room temperature.

3. Results and discussion

3.1. Microstructural evolution during heating

The simultaneous measurement of DSC and ND spectra allows us to distinguish the different phases appearing during heating. Figure 1 shows the DSC measurement at a heating rate of 8 °C min^{-1} corresponding to the as-quenched sample. Four different peaks, indicated by open arrows, can be observed, two of them exothermic and the other two endothermic.

A series of ND spectra, measured *in situ* during heating at the same rate, allows us to identify the different precipitation stages. Figure 2 shows ND spectra measured at different

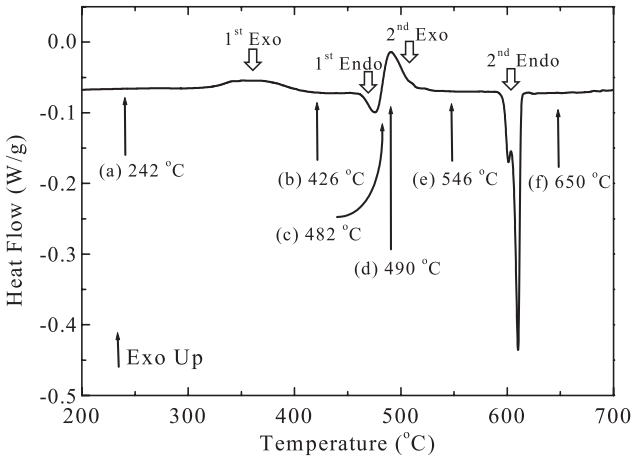

Figure 1. DSC measurement of the as-quenched sample at 8 °C min^{-1}. Black arrows indicate the stages corresponding to the diffraction spectra of figure 2.

temperatures corresponding to particular stages of the DSC curve (indicated by black arrows in figure 1). The full line represents the corresponding Rietveld refinement. At low temperatures, below the first exothermic peak (1st Exo) temperature, only the β_3 ordered phase ($L2_1$) [15] is present in the alloy, as shown in figure 2(a). After heating through the exothermic process, the alloy is composed of both the β_3 phase and the γ_1 phase, figure 2(b). Then the 1st Exo peak can be associated to the primary $\beta_3 \rightarrow \gamma_1$ precipitation process. Above 460 °C two simultaneous processes take place during heating: the disordering of the metastable β_3 phase to a B2 structure (β_2 phase) and the precipitation of γ_1 and α stable phases during the eutectoid decomposition $\beta \rightarrow \alpha + \gamma_1$. Figures 2(c) and (d) show the diffraction patterns measured at 482 and 490 °C, respectively. In these patterns, the reflections corresponding to three different phases identified as β, α and γ_1 are shown. In particular, the (111) reflection of the β_3 phase ($L2_1$ structure) observed at 482 °C disappears at 490 °C, where the β phase is only ordered (β_2) at the nearest neighbours (B2 structure). The loss of the order at the next-nearest neighbours implies a half reduction of the cell parameter. Then, the second order–disorder transition temperature must be located between both temperatures in agreement with order–disorder transition temperatures for the β phase in Cu–Al–Ni [5]. As a consequence, the first endothermic peak (1st Endo) is linked to the loss of the next-nearest neighbours' order, the $L2_1$ to B2 transition. The last part of the disordering process overlaps the $\beta \rightarrow \alpha + \gamma_1$ eutectoid decomposition, the second exothermic peak (2nd Exo), as deduced from the presence of α phase in figures 2(c) and (d). Figure 2(f) corresponds to the end of the $\beta \rightarrow \alpha + \gamma_1$ eutectoid decomposition. The present phases are $\alpha + \gamma_1$ with precipitated mass fractions of $f_m(\alpha) = 25 \pm 1\%$ and $f_m(\gamma_1) = 75 \pm 1\%$. The spectrum shown in figure 2(f), obtained after the second endothermic peak (2nd Endo), indicates that this process is associated with the dissolution of the eutectoid phases at the eutectoid decomposition temperature in the equilibrium phase diagram [4]. Then, the remaining phases are the disordered β phase and the γ_1 primary phase, as indicated in figure 2(f).

A summary is shown in figure 3. The β phase is stable below 300 °C and decomposes first into the γ_1 phase above 300 °C according to a pro-eutectic process. This primary $\beta_3 \rightarrow \gamma_1$ precipitation process limits the high-temperature applications of these alloys since the behaviour of the MT changes with the apparition of the early precipitates, as will be analysed

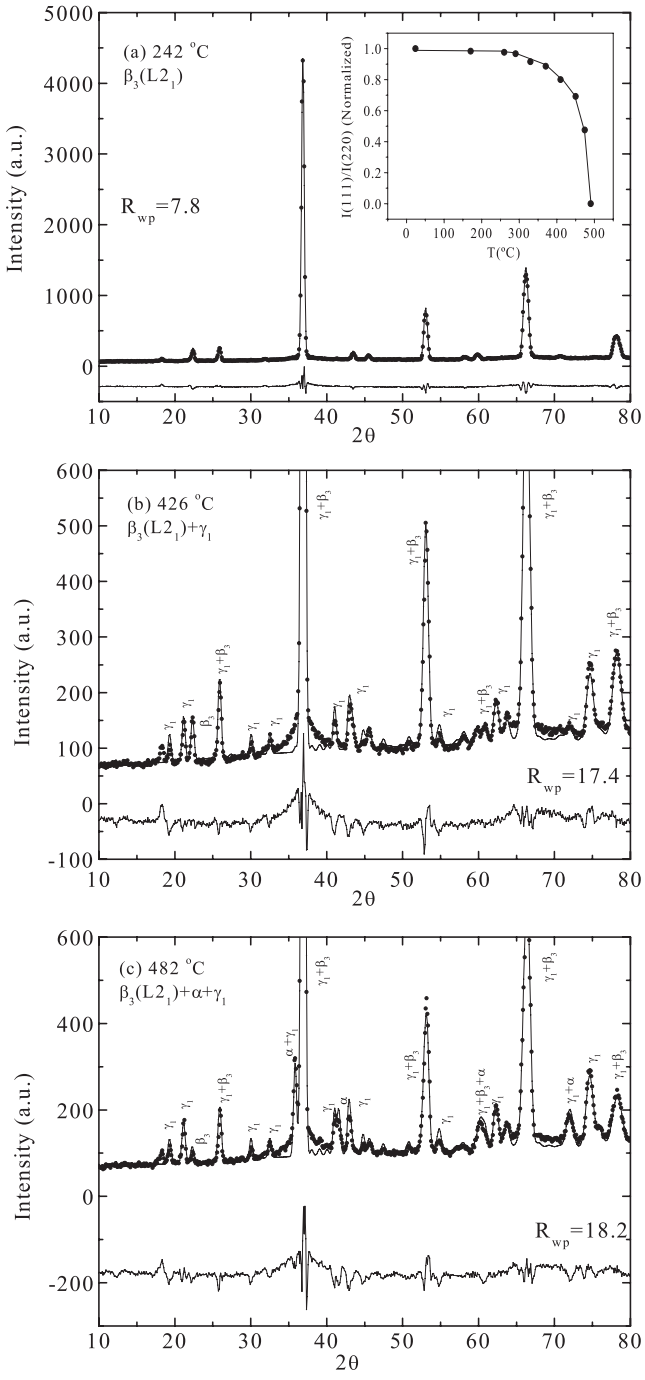

Figure 2. Neutron diffraction spectra measured at different temperatures *in situ* during heating at 8 °C min^{-1} (dots) and Rietveld refinement (full line). Peaks of α, β and γ_1 phases are labelled. The inset in (a) shows the normalized relative intensity of the (111) superlattice reflection compared to the fundamental (220) reflection as a function of temperature.

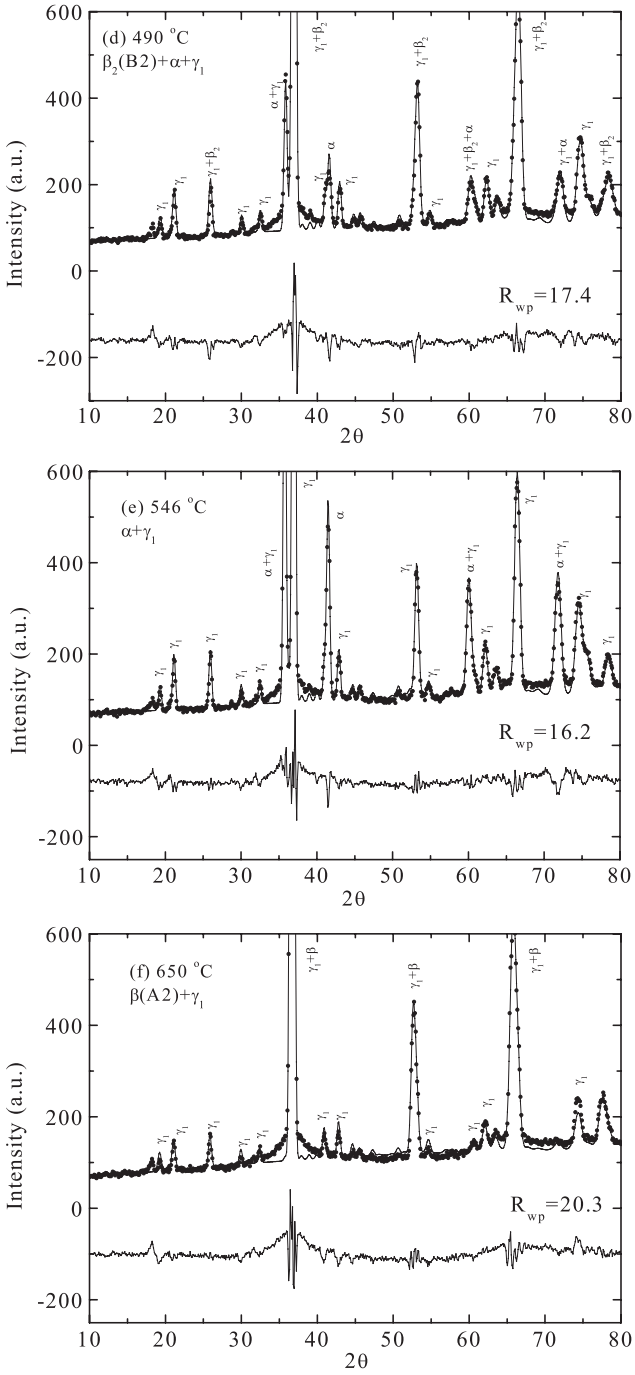

Figure 2. (Continued).

in the second part of this work. Between 300 and 440 °C, the mass fraction of β_3 and γ_1 phases follows a sigmoid curve. The eutectoid decomposition takes place above 440 °C and

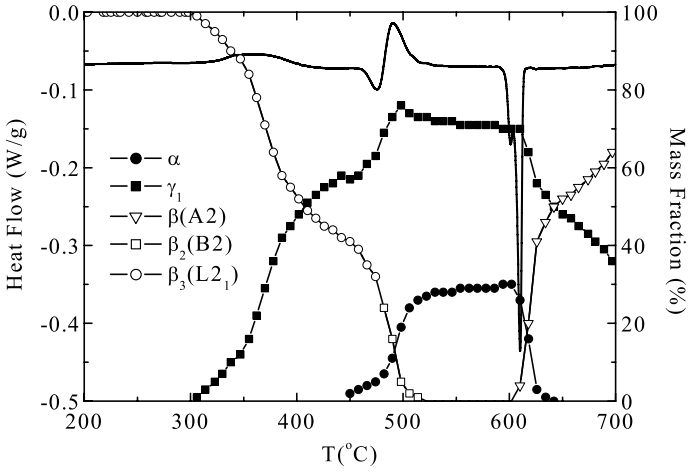

Figure 3. Precipitated mass fraction of the different phases and their evolution during heating. Black labels: ■ γ_1 phase, ● α phase. White labels: ○ β_3 phase ($L2_1$), □ β_2 phase (B2) and ▽ β phase (disordered). The DSC (full line) is also shown for comparison.

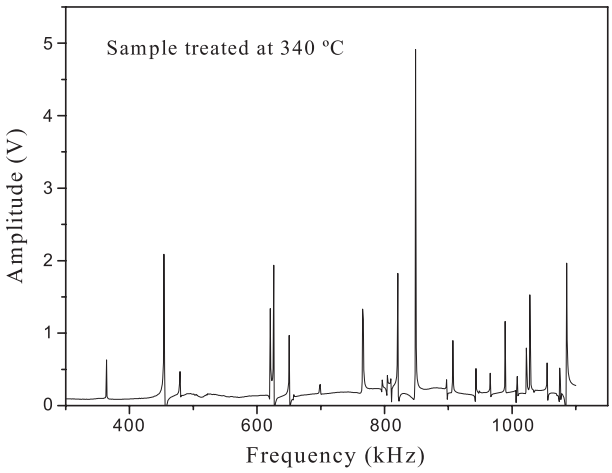

Figure 4. Room-temperature RUS spectrum corresponding to the sample thermally treated at 340 °C.

the β_3 phase transforms to β_2 at 490 °C, disappearing at the end of this stage. Finally, the full disappearance of the α phase can be observed to be linked to the dissolution of the eutectoid phases. The remaining phases above 640 °C are the disordered β phase and the γ_1 primary phase that disappears at around 800 °C. Thus, this temperature is the stability limit of the β phase, as has been checked by differential thermal analysis (DTA).

Since the γ_1 precipitation limits the high-temperature applications, the influence of the early stage of decomposition on the elastic behaviour of the alloy has been studied. The samples were analysed after different thermal treatments according to the results shown in figure 3. In the RUS technique the elastic constants are determined from the fitting of the experimental resonance frequencies to the theoretical spectrum of the sample. That is, figure 4 shows the room-temperature resonance spectrum corresponding to the sample thermally treated

Table 1. Experimental frequency resonances, theoretical values obtained after refinement and the error corresponding to a sample treated at 340 °C and measured at room temperature (the elastic constants of this sample are indicated). The theoretical sensitivities, $A = (2C_{11}/f_n)(\partial f_n/\partial C_{11})$ and $B = (2C_{44}/f_n)(\partial f_n/\partial C_{44})$ of the different resonances are also shown. (Note: C_{11}—180.31 GPa and C_{44}—41.91 GPa.)

Frequency (MHz) (experimental)	Frequency (MHz) (theoretical)	Error (%)	$A = 2C_{11}/f\cdot\partial f/\partial C_{11}$	$B = 2C_{44}/f\cdot\partial f/\partial C_{44}$
0.363 964	0.362 568	−0.38	0.00	1.00
0.454 294	0.454 674	0.08	0.10	0.90
0.479 119	0.477 871	−0.26	0.10	0.90
0.620 941	0.619 229	−0.28	0.02	0.98
0.626 386	0.626 079	−0.05	0.06	0.94
0.650 691	0.651 211	0.08	0.00	1.00
0.657 778	0.659 046	0.19	0.02	0.98
0.698 799	0.699 571	0.11	0.03	0.97
0.766 246	0.767 546	0.17	0.02	0.98
0.796 366	0.796 605	0.03	0.14	0.86
0.804 054	0.804 126	0.01	0.03	0.97
0.810 541	0.809 107	−0.18	0.04	0.96
0.820 991	0.819 647	−0.16	0.03	0.97
0.848 669	0.849 803	0.13	0.08	0.92
0.897 618	0.895 458	−0.24	0.01	0.99
0.906 987	0.904 269	−0.30	0.03	0.97
0.943 243	0.944 563	0.14	0.03	0.97
0.948 709	0.952 642	0.41	0.01	0.99
0.966 126	0.966 813	0.07	0.05	0.95
0.989 345	0.992 781	0.35	0.07	0.93
1.006 310	1.007 453	0.11	0.15	0.85
1.008 070	1.010 483	0.24	0.08	0.92
1.022 880	1.022 085	−0.08	0.09	0.91
1.027 960	1.024 034	−0.38	0.12	0.88
1.028 680	1.027 783	−0.09	0.23	0.77
1.034 700	1.033 220	−0.14	0.11	0.89
1.055 320	1.054 981	−0.03	0.06	0.94
1.070 570	1.073 372	0.26	0.09	0.91
1.075 020	1.076 328	0.12	0.15	0.85
1.076 400	1.076 838	0.04	0.00	1.00

at 340 °C. The experimental resonances, the theoretical values obtained after refinement and the error are shown in table 1. An RUS eigenmode may depend on several elastic constants and the eigenfrequencies $f_n = f_n(C_{11}, C_{44})$ have different sensitivities to C_{ij} (isotropic crystals) [30]. In order to see the influence of the different elastic constants in a particular vibration mode, table 1 also shows the different theoretical sensitivities of the resonance frequencies, $A = (2C_{11}/f_n)(\partial f_n/\partial C_{11})$ and $B = (2C_{44}/f_n)(\partial f_n/\partial C_{44})$ corresponding to the measured vibration modes at room temperature (sample treated at 340 °C). The B value is much higher than A for all the resonance frequencies, which means that the vibrational behaviour in the frequency range studied is mainly controlled by the C_{44} elastic constant. The refined C_{11} and C_{44} elastic constants allow us to determine the values of the Young modulus E and shear modulus G using

$$E = C_{44}\frac{3C_{11} - 4C_{44}}{C_{11} - C_{44}} \qquad \text{and} \qquad G = C_{44}.$$

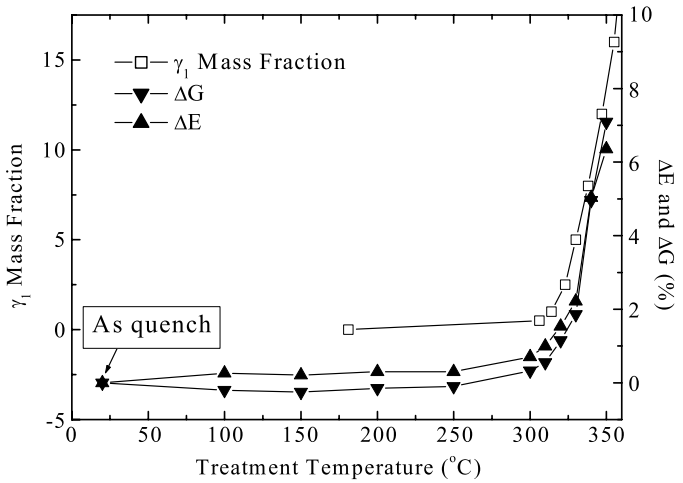

Figure 5. Evolution of the relative values of E and G and the γ_1 precipitated mass fraction at the early stage of precipitation (below 350 °C) as a function of the maximum thermal treatment temperature.

The values of the elastic constants of the β_3 phase measured at room temperature in the as-quenched state are $E = 108.0 \pm 0.2$ GPa and $G = 39.95 \pm 0.05$ GPa. These results are in very good agreement with isotropic elastic constants obtained averaging the single-crystal values for these alloys using the Hill approximation, $E = 110$ GPa and $G = 41$ GPa from [32], $E = 106$ GPa and $G = 39$ GPa from [33].

Figure 5 shows the evolution of the relative values of E and G and the γ_1 precipitated mass fraction at the early stage of precipitation as a function of the maximum thermal treatment temperature. Both elastic constants increase in the same way with temperature. Higher values for the elastic constants of the γ_1 phase than for the β_3 phase are expected, taking into account the intermetallic character of the γ brass. The increase of the effective values of elastic constants corresponding to a mixture of both phases is explained from the formula of the Hashin–Shtrikman bound in the limit of low volume fraction $f \ll 1$ [34].

3.2. Martensitic transformation

As has been pointed out in previous paragraphs, the precipitation of the primary γ_1 phase limits the high-temperature applications of these alloys since the MT behaviour degrades with precipitation. In contrast, during the first stages of the precipitation, previously to the degradation of the transformation, the characteristic of the MT can be tailored without losing the thermoelastic character [19–22].

To study the influence of pre-heating temperature on the MT characteristics, cooling–heating DSC cycles through the MT after heating up to different temperatures were carried (figure 6). The forward MT in the as-quenched state presents only a peak composed by a high-temperature side formed by a succession of sharp peaks and a continuous low-temperature side. In contrast, the reverse MT shows two peaks. This behaviour is characteristic of a mixed $\beta \rightarrow \gamma' + \beta'$ MT [35]. The presence of two peaks during the reverse MT is due to the different transformation hysteresis of both transformations. The low-temperature peak is linked to the $\beta' \rightarrow \beta$ retransformation and the high-temperature one to the $\gamma' \rightarrow \beta$. Different kinds of MT have been observed in single-crystal Cu–Al–Ni SMAs depending on

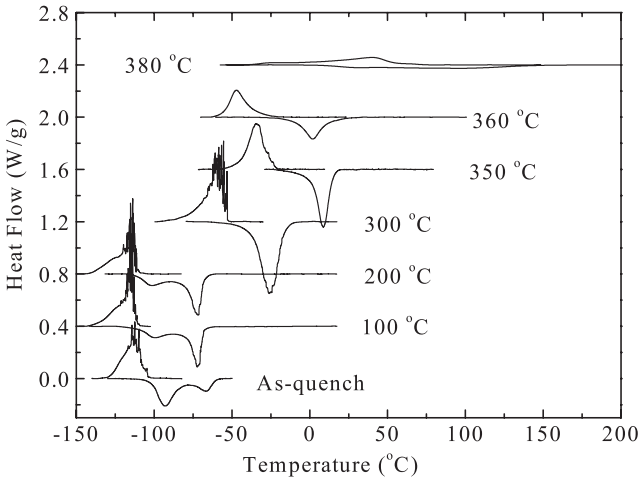

Figure 6. Cooling–heating DSC cycles through the MT after heating up to different temperatures (indicated in the figure).

the alloy concentration, as evidenced in an MT–alloy composition map [35]. In summary, the increase of the aluminium content (at constant Ni) modifies the type of induced martensite from $\beta \rightarrow \beta'$ to $\beta \rightarrow \gamma'$. Between these two regions, there is an intermediate composition range where a mixed $\beta \rightarrow \gamma' + \beta'$ MT is thermally induced. The alloy composition falls into the $\beta \rightarrow \gamma'$ region but the measured DSC shows a $\beta \rightarrow \gamma' + \beta'$ transformation path. However, in this work the alloy is not a single crystal. In contrast, the HIP technique allows one to obtain polycrystalline alloys with an average grain size of 50 μm. The stored elastic stresses induced during quenching modify the energy balance of the MT, and the $\beta \rightarrow \gamma' + \beta'$ transformation is promoted for this concentration. Thus, the effect of elastic stresses can be described as a shift of the mixed $\beta \rightarrow \gamma' + \beta'$ MT composition range in the MT–alloy composition map to the region of higher aluminium concentration. For pre-heatings below 300 °C there are no changes in the forward transformation. During the reverse transformation the heat associated with the first (γ_1' reversion) and second (β_1' reversion) endothermic peaks decreases and increases, respectively. Then, the induced γ_1' martensite fraction increases with respect to the fraction of β_1' martensite as long as the treatment temperature increases. The MT evolves from a mixed $\beta \rightarrow \gamma' + \beta'$ to a $\beta \rightarrow \gamma'$ single MT, increasing the heating limit temperature. Above 200 °C only one peak is observed during the reverse transformation. In order to check this point, figure 7 shows the ND spectrum corresponding to a sample aged for 4 h at 190 °C. The spectrum corresponds to a single γ' martensite. The full line represents the Rietveld refinement assuming a single γ' martensite with a *Pmmn* space group and cell parameters $a = 5.389(2)$ Å, $b = 4.216(1)$ Å and $c = 4.357(1)$ Å. Table 2 shows the refined atomic position of the different atoms.

Figure 8 shows the M_s and A_f temperatures of the MT versus the heating limit temperature and their associated hysteresis (two different hystereses are shown below 300 °C, that correspond to the $\beta \rightarrow \beta'$ and to the $\beta \rightarrow \gamma'$). A slight increase below 300 °C and a higher increase above 300 °C are observed in the MT temperatures. The hysteresis shows first a decrease in both the $\beta \leftrightarrow \gamma'$ and $\beta \leftrightarrow \beta'$ cycles and then an increase associated with the $\beta \leftrightarrow \gamma'$ MT (above 300 °C only a single $\beta \rightarrow \gamma'$ MT appears, figure 6). The elastic stresses stored during quenching play an important role. The as-quenched alloy has an $L2_1$ order,

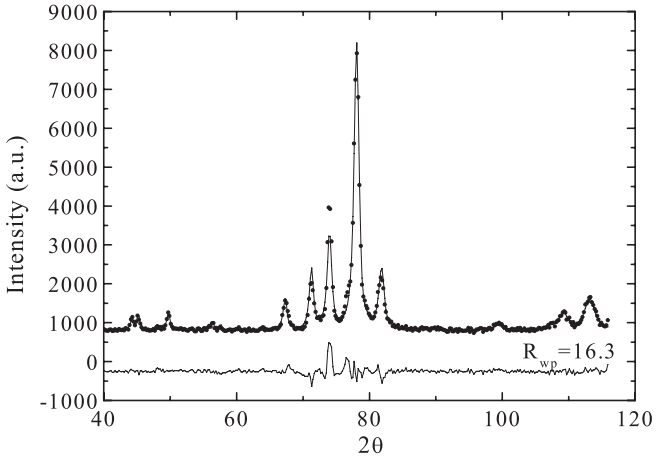

Figure 7. Neutron diffraction spectrum corresponding to a sample aged for 4 h at 190 °C. The full line represents the Rietveld refinement assuming a single γ' martensite.

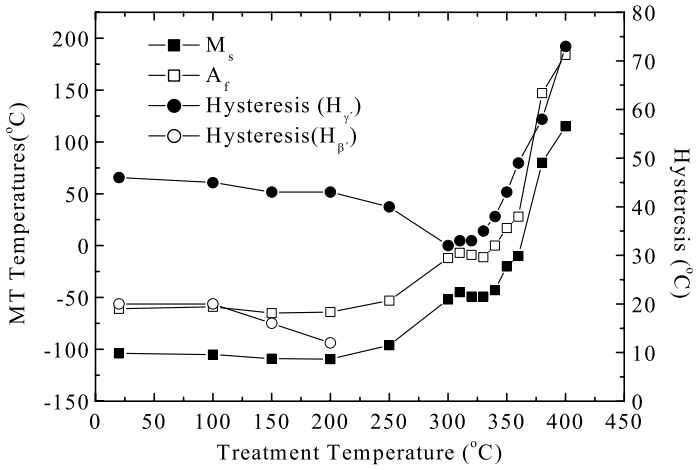

Figure 8. Evolution of the martensite and austenite start temperatures, (M_s) and (A_f) respectively and their associated hysteresis (two different hystereses are shown below 300 °C, that correspond to the $\beta \rightarrow \beta'$ and to the $\beta \rightarrow \gamma'$) after heating to the temperatures indicated in the x axis.

Table 2. Atomic position and occupation factors of the γ' martensite refined in space group $Pmmn$. Only the values given as decimals were refined.

Position	Name	x	y	z	Occupation
2a	Al1	1/4	1/4	0.276(7)	0.25(1)
2a	Cu1	1/4	1/4	0.276(7)	0.00(1)
2b	Al2	1/4	3/4	0.686(4)	0.02(1)
2b	Cu2	1/4	3/4	0.686(4)	0.24(1)
4f	Ni3	0.000(2)	1/4	0.810(2)	0.08(4)
4f	Cu3	0.000(2)	1/4	0.810(2)	0.42(4)

and no changes were detected in the structure during heating [15, 16]. DSC measurements in this temperature range do not show any detectable thermal process. Nevertheless, the

inset in figure 2(a) shows the normalized relative intensity of the (111) superlattice reflection (characteristic of an $L2_1$ structure) compared to the fundamental (220) reflection as a function of temperature. The decrease of this relative value is a consequence of the reduction in the $L2_1$ order parameter near the second-order transition. Below 200 °C the order parameter seems to be constant. Then, below 200 °C, the increase of the MT temperatures, the reduction associated to hysteresis and the change from a mixed $\beta \rightarrow \gamma' + \beta'$ MT to a single $\beta \rightarrow \gamma'$ MT must be associated with the relaxation of internal stresses and/or to the recovery on quenched-in defects. Neutron diffraction does not detect any order increase during heating given that it could be masked by the reduction in the order parameter near the order–disorder transition. Then, the increase in the transformation temperatures and the reduction in the hysteresis in the range 200–300 °C could be associated to a slight increase in the order degree. The higher ability of β' martensite to accommodate the stresses explains the transformation path in a mixed $\beta \rightarrow \gamma' + \beta'$ MT [36]. The β phase starts to transform to γ' martensite but, at an intermediate temperature when the internal stresses in the remaining β phase reach a certain value, this transformation stops and the β phase finishes transforming to β' martensite. Although this martensite has higher transformation strain it easily forms self-accommodant groups of variants and the internal stresses are better accommodated. The difference in the thermograms for both transformations is due to the different growing kinetics of both martensites. The β' martensite has a more thermoelastic and smooth behaviour during transformation. In contrast, the γ' MT takes place by avalanches. The presence of two peaks during the reverse MT is due to the different transformation hysteresis of both transformations. Above 300 °C the start of the γ_1 precipitation marks the limit between two stages in the behaviour of the MT and hysteresis (figure 6). Nevertheless, focusing in the range between 300 and 350 °C, the MT temperatures seems to keep constant and the hysteresis increases slightly. This behaviour is explained by the presence of coherent precipitates at the early stage of the γ_1 precipitation that modify the elastic and frictional energy terms in the energy balance of the MT [21]. For higher temperatures an increase of both MT temperatures and hysteresis is detected. In this last range of temperatures the chemical energy changes dominate the MT kinetics due to the composition changes in the β matrix. The precipitates deplete the β matrix of aluminium, shifting the transformation to higher temperatures [35], and also create composition gradients which increase the MT interval. The transformation enthalpy for the sample aged below 300 °C is around 4.3 J g^{-1}, increasing to 6 J g^{-1} above 300 °C when the decomposition starts. This increase of transformation enthalpy before decomposition is probably due to the increase of transformation temperatures with the heat treatments, resulting in nearly constant transformation entropy. As soon as the γ_1 precipitation proceeds, the enthalpy progressively reduces, indicating a lower transformed volume fraction.

Focusing on the stage previous to decomposition, figure 9 shows the evolution of the γ' volume fraction and the C_{44} elastic constant as a function of the preheat treatment below 250 °C. Only C_{44} has been considered due to the higher accuracy in the determination of this elastic constant from RUS measurements (see table 1; a higher sensitivity of the resonance frequencies on C_{44} implies a higher weight of this elastic constant on the fitting). The γ' volume fraction increases from 20% for the as-quenched alloy to 100% after heating to 250 °C. In contrast, the C_{44} elastic constant first decreases and then increases for treatments above 150 °C. This means that two different mechanisms are involved in this previous stage. The usual increase of the elastic constants under applied stresses has been confirmed from the measurements of the third-order elastic constants of the β phase in Cu–Al–Ni SMAs [37]. Thus, a relaxation of internal stresses must be expected to be linked to the initial decrease of C_{44} elastic constant. As pointed out above, the kind of induced martensite changes from γ' to β' due to the stresses stored in the remnant parent phase. The relaxation of internal stresses induced during quenching reduces

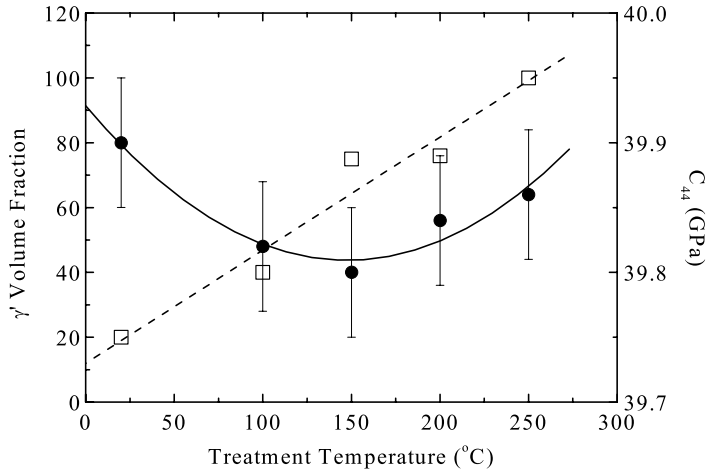

Figure 9. Evolution of the γ' volume fraction and the C_{44} elastic constant as a function of the preheat treatment below 250 °C.

the level of stresses of the β phase and consequently more volume fraction of transformed γ' martensite is necessary to achieve the threshold of stored stresses to induce β' martensite. As a result, the relaxation of internal stresses stabilizes the γ' phase, increasing and decreasing the transformed γ' and β' volume fraction, respectively. In contrast, the C_{44} increase above 150 °C could be associated with the recovery of quenched-in defects and/or to a slight increase of the order degree.

4. Conclusions

The β phase decomposition processes during heating and their influence in the MT have been studied in a Cu–14.37Al–4.2Ni (wt%) alloy produced by HIP. The pro-eutectoid γ_1 precipitation, the $L2_1$ to B2 disordering process and the eutectoid decomposition have been observed during heating, followed by its subsequent dissolution at higher temperatures. The γ_1 precipitation (above 300 °C) limits high-temperature applications. Resonant ultrasound spectroscopy has been used to determine the increase of the E and G elastic constants during the early stage of γ_1 decomposition. Finally, the evolution of the kind of induced martensite, hysteresis and transformation temperatures has been analysed during the precipitation of γ_1 phase. The elastic stresses stored during quenching and the slight change of the order degree play an important role in the MT evolution below 300 °C. At higher temperatures, the γ_1 precipitation process induces an increase of the MT transformation temperatures.

Acknowledgments

This work has been carried out with the financial support of the Spanish 'Ministerio de Ciencia y Tecnología' (Project number MAT2003-05243). The 'Servicio de apoyo a la investigación' of the Universidad Pública de Navarra is acknowledged for the DSC measurements (TA 2920 equipment). The Institute Laue-Langevin, D20 and D1B installations, (Grenoble, France) is acknowledged for the allocated neutron beamtime (Exp. 5-25-73 and CRG 701).

References

[1] Gandhi M V and Thompson B S 1992 *Smart Materials and Structures* (London: Chapman and Hall)
[2] Funakubo H 1987 *Shape Memory Alloys* (New York: Gordon and Breach)
[3] Delaey L 1991 *Phase Transformations in Materials* (Weinheim: VCH) chapter 6
[4] Petzow E G and Effenberg E 1991 *Ternary Alloys* vol 4 (Weinheim: VCH)
[5] Recarte V, Lambri O A, Pérez-Sáez R B, Nó M L and San Juan J 1997 *Appl. Phys. Lett.* **70** 3513
[6] Pérez-Landazábal J I, Recarte V, Pérez-Sáez R B, Nó M L, Campo J and San Juan J 2002 *Appl. Phys. Lett.* **81** 1794
[7] Van Humbeeck J, Van Hulle D, Delaey L, Ortín J, Seguí C and Torra V 1987 *Mater. Trans. JIM* **28** 383
[8] Sakamoto H and Shimizu K 1989 *Iron Steel Inst. Japan Int.* **29** 395
[9] Recarte V, Pérez-Sáez R B, Nó M L and San Juan J 1999 *J. Mater. Res.* **14** 2806
[10] Bouabdllah M and Cizeron G 1998 *Eur. Phys. J. Appl. Phys.* **1** 163
[11] Olson G B and Cohen M 1975 *Scr. Metall.* **9** 1247
Olson G B and Cohen M 1977 *Scr. Metall.* **11** 345
[12] Warlimont H and Delaey L 1974 *Prog. Mater. Sci.* **18** 1
[13] Ortín J and Planes A 1988 *Acta Metall.* **36** 2417
Ortín J and Planes A 1989 *Acta Metall.* **37** 1433
[14] Recarte V, Pérez-Landazábal J I, Rodríguez P P, Bocanegra E H, Nó M L and San Juan J 2004 *Acta Mater.* **52** 3941
[15] Recarte V, Pérez-Landazábal J I, Campo J, Pérez-Sáez R B, Nó M L and San Juan J 2003 *J. Physique* IV **112** 605
[16] Pérez-Landazábal J I, Recarte V, Nó M L and San Juan J 2004 *Physica* B **350** e1007
[17] Cahn R W and Haasen P 1996 *Physical Metallurgy* (Amsterdam: Elsevier Science) chapter 3
[18] Pérez-Landazábal J I, Recarte V, Nó M L and San Juan J 2003 *Intermetallics* **11** 927
[19] Rodriguez P and Guenin G 1990 *Mater. Sci. Eng.* A **129** 273
[20] Duktkiewicz J, Pons J and Cesari E 1992 *Mater. Sci. Eng.* A **158** 119
[21] Cesari E, Pons J and Chandrasekaran M 1994 *Trans. Mater. Res. Soc. Japan* **18B** 903
[22] Zarubová N, Gemperle A and Novák V 1997 *Mater. Sci. Eng.* A **222** 166
[23] Miyazaki S, Otsuka K, Sakamoto H and Shimizu K 1981 *Trans. Japan Inst. Met.* **4** 224
[24] San Juan J, Pérez-Sáez R B, Recarte V, Nó M L, Caruana G, Lieblich M and Ruano O A 1995 *J. Physique* IV **5** 919
[25] Pérez-Sáez R B, Recarte V, Nó M L, Ruano O A and San Juan J 2000 *Adv. Eng. Mater.* **2** 49
[26] Rietveld H M 1969 *J. Appl. Crystallogr.* **2** 65
[27] Young R A 1993 *The Rietveld Method* (Oxford: Oxford Science Publications)
[28] Rodriguez-Carvajal J 1993 *Physica* B **192** 55
[29] Rodriguez-Carvajal J 2001 *FullProf 2000* a computer program
[30] Migliori A and Sarrao J L 1997 *Resonant Ultrasound Spectroscopy* (New York: Wiley)
[31] Leisure R G and Willis F A 1997 *J. Phys.: Condens. Matter* **9** 6001
[32] Recarte V, Pérez-Landazábal J I, Nó M L and San Juan J 2004 *Mater. Sci. Eng.* A **370** 488
[33] Mañosa Ll, Jurado M, Planes A, Zarestky J, Lograsso T and Stassis C 1994 *Phys. Rev.* B **49** 9969
[34] Recarte V, Pérez-Landazábal J I and Sánchez-Alarcos V 2005 *Appl. Phys. Lett.* **86** 231903
[35] Recarte V, Pérez-Sáez R B, Bocanegra E H, Nó M L and San Juan J 2002 *Metall. Mater. Trans.* A **33** 2581
[36] Van Humbeeck J, Van Hulle D, Delaey L, Ortín J, Seguí C and Torra V 1987 *Trans. Japan Inst. Met.* **28** 383
[37] González-Comas A and Mañosa Ll 1996 *Phys. Rev.* B **54** 6007